

# Electromagnetic Response of a Half-Filled Chern Band near Topological Criticality

Xinlei Yue,<sup>1</sup> Fabian Pichler,<sup>2,3</sup> Michael Knap,<sup>2,3</sup> and Ady Stern<sup>1</sup>

<sup>1</sup>*Department of Condensed Matter Physics, Weizmann Institute of Science, Rehovot, Israel 7610001*

<sup>2</sup>*Technical University of Munich, TUM School of Natural Sciences, Physics Department, 85748 Garching, Germany*

<sup>3</sup>*Munich Center for Quantum Science and Technology (MCQST), Schellingstr. 4, 80799 München, Germany*

We evaluate electromagnetic-response observables in a half-filled Chern band, across a topological phase transition between a composite Fermi liquid (CFL) and a Fermi liquid (FL) phase. While a sharp gapped plasma mode exists deep in the CFL phase, we demonstrate that it is damped near the proposed continuous phase transition between CFL and FL. This plasmon-damping phenomenon originates from emergent gauge fields and a Dirac-fermion-like spectrum. Similar features also occur in other continuous deconfined topological phase transitions, such as the Laughlin to superfluid transition in a bosonic system. In particular, this damping behavior extends over a finite range across the phase boundary, and, hence, we expect it to persist even when the transition is weakly first-order. Furthermore, we analyze the behavior of the Drude weight, the wavevector-dependent conductivity, and the chiral mirror effect across these topological phase transitions.

**Introduction.**—Striking experimental developments in two-dimensional materials have opened new avenues for realizing phases with topological order. Notably, fractional Chern insulators (FCIs) [1–7] have been discovered at zero magnetic field in twisted MoTe<sub>2</sub> [8–13] and rhombohedral graphene [14–17], providing concrete platforms for studying strongly correlated phases in Chern bands. The exceptional tunability and control of these systems have enabled the exploration of rich phase diagrams and sparked theoretical interest in continuous topological transitions between fractionalized states [18–45]. A particularly intriguing example is the transition between a composite Fermi liquid (CFL) [46] and a Fermi liquid (FL), taking place in a half-filled Chern band as the ratio of interaction strength to band width is varied [47–50]. Recent experiments [9, 17] have already observed the CFL and FL phases nearby in parameter space, although at low temperature they seem to be separated by an intermediate phase, potentially an insulating state or extended quantum Hall state. Theoretically, the CFL to FL phase transition has attracted further interest since it is proposed to be possibly a deconfined topological phase transition (TPT) beyond the Landau phase transition paradigm [23, 31]. Numerical works [27, 36–38] have provided strong evidence for a continuous deconfined TPT between a bosonic Laughlin state and a superfluid phase, which is closely related to the CFL to FL transition in the deconfined TPT framework. However, to develop a better experimental understanding of these exotic phase transitions, it is pertinent to identify their unique signatures.

In this work, we examine the evolution of the electromagnetic response across a transition between a CFL and an FL, focusing on identifying characteristics of the two phases. These characteristics include the plasma mode, the Drude weight, the conductivity at non-zero wave vector, and chiral mirroring. Their evolution is controlled by two key ingredients of deconfined TPTs: emergent gauge fields and a Dirac fermion spectrum. We analyze some of these signatures also in other deconfined TPTs, including the Laughlin-superfluid transition [25] and the Laughlin-insulator-superfluid (CFL-insulator\*-FL) transition [23, 25]. While we assume a con-

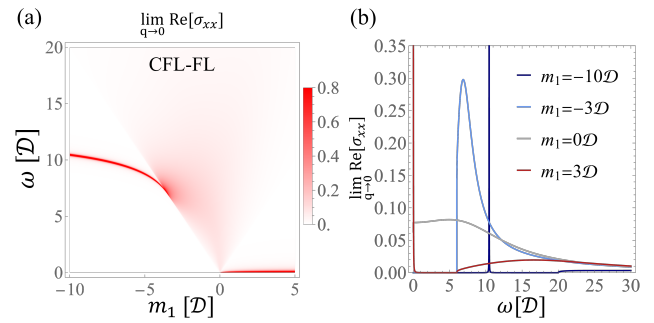


FIG. 1. *Damping of the plasmon mode near a CFL-FL topological phase transition.* (a) Absolute value of the real part of the conductivity  $\sigma_{xx}(\omega)$  in the vicinity of the CFL ( $m_1 < 0$ ) to FL ( $m_1 > 0$ ) transition in the long wavelength limit,  $q \rightarrow 0$ . The plasma mode has a long lifetime at large  $|m_1|$  but is damped when it enters the particle-hole continuum of the emergent Dirac fermions near the deconfined topological phase transition (the fan is determined by  $\omega > 2|m_1|$ ). (b) Line cuts at different masses  $m_1$ . The energies are measured in units of the parton Drude weight  $\mathcal{D}$ .

tinuous transition in our calculations, we expect qualitatively similar behavior to appear even if the deconfined TPTs become weakly first-order. Thereby, we establish unique signatures that can be probed experimentally using quickly developing THz spectroscopy techniques; see e.g. Refs. [51–55].

*Plasmon damping near topological criticality.*—The CFL phase in a Chern band [48–50, 56] may be described by composite fermion theory. In that theory, the relevant quasiparticle is the Composite Fermion (CF), which is composed of an electron and two flux quanta [57, 58]. The resistivity of the electrons is given by

$$\rho_e = \rho_{\text{CF}} + \rho_{\text{cs}} \quad (1)$$

where

$$\rho_{\text{CF}} = \begin{bmatrix} -\frac{i\omega}{\mathcal{D}} & 0 \\ 0 & -\frac{i\omega}{\mathcal{D}} \end{bmatrix} \quad \text{and} \quad \rho_{\text{cs}} = \begin{bmatrix} 0 & 4\pi \\ -4\pi & 0 \end{bmatrix} \quad (2)$$

are the resistivity of the FL formed by the CF, and the resistivity generated by the motion of the two flux quanta (resulting

from the Chern-Simons (CS) term of the topological field theory), respectively. Here, the components of the matrix refer to the spatial  $x$ - and  $y$ -directions, and we set  $e = \hbar = c = 1$ , such that  $4\pi$  corresponds to  $2h/e^2$ . For now, we focus on zero momentum  $q = 0$ , and neglect the Hall conductivity of the composite fermions, arising from the Berry curvature in their band. Furthermore, we assume a perfectly clean system. Then, the composite fermions have a Drude weight  $\mathcal{D} \equiv \lim_{\omega \rightarrow 0} i\omega \rho_{\text{cf}}^{-1}$ . These simplifications will be relaxed at a later stage of our analysis.

The plasmon corresponds to the zero determinant of the electron resistivity tensor  $\rho_e$ . Combining Eqs. (1) and (2), we see that the plasmon is gapped, at  $\omega_p = 4\pi\mathcal{D}$ . The gapping of the plasma mode is a remarkable property of the CFL, which comes hand in hand with the vanishing of the electronic Drude weight,  $\mathcal{D}_e = \lim_{\omega \rightarrow 0} i\omega \sigma_{e,xx}$ , with  $\sigma_e \equiv \rho_e^{-1}$  being the electronic conductivity. By contrast, on the FL side, the plasma mode is gapless at  $q = 0$ , and follows a dispersion  $\omega \propto q^{1/2}$ .

Our analysis of the transition between CFL and FL builds on the pioneering work of Barkeshli and McGreevy [23], which was followed up by Song, Zhang, and Senthil [31]. We replace the resistivity matrix of the flux quanta  $\rho_{\text{cs}}$  by the sum of two resistivity matrices,  $\rho_1, \rho_2$ . These resistivity matrices describe particles, i.e., partons, that fully fill two Chern bands, with Chern numbers  $\mathcal{C}_1, \mathcal{C}_2$ . Formally, this is achieved by decomposing the electron into three partons,  $c = f d_1 d_2$ , where  $f$  corresponds to the CF and the combined  $d_1$  and  $d_2$  to the two flux quanta in the CF description. This approach allows us to treat these flux quanta dynamically. The dynamics is captured by three Lagrangians of the partons, which are coupled to one another by two gauge fields  $a_\mu, b_\mu$ , with  $\mu = 0, x, y$ . We use bold-faced  $\mathbf{a}, \mathbf{b}$  for the spatial components of  $a_\mu, b_\mu$ . The  $d_1$  partons are coupled to the gauge field  $a_\mu$ , the  $d_2$  partons are coupled to  $b_\mu$ , and the  $f$  partons are coupled to  $-a_\mu - b_\mu$ . When  $a_\mu$  and  $b_\mu$  are integrated out, the density and currents of  $f$  are enforced to equal those of  $d_1$  and  $d_2$ . The sum of the three Lagrangians is then,

$$\mathcal{L} = \mathcal{L}_{\text{cf}}[f^\dagger, f, A_\mu - a_\mu - b_\mu] + \mathcal{L}_1[d_1^\dagger, d_1, a_\mu] + \mathcal{L}_2[d_2^\dagger, d_2, b_\mu] \quad (3)$$

with

$$\mathcal{L}_1 = d_1^\dagger(\partial_t - a_0 - \mu)d_1 - H_1(d_1^\dagger, d_1, \mathbf{a}). \quad (4)$$

Here,  $H_1$  is the Hamiltonian of the  $d_1$  partons. Similar expressions hold for  $\mathcal{L}_2$  and  $\mathcal{L}_{\text{cf}}$ . Crucially, only the  $f$  partons couple to the electromagnetic vector potential  $A_\mu$ . Thus, the charge density is  $f^\dagger f$ . The physical electronic resistivity is given by the Ioffe-Larkin rule to be the sum of the resistivities of the three partons (see Eqs. (13) and (14) in the End Matter for a derivation)

$$\rho_e = \rho_{\text{cf}} + \rho_1 + \rho_2. \quad (5)$$

For the CFL phase, we have  $\mathcal{C}_1 = \mathcal{C}_2 = 1$ , such that the resistivity of the partons in the filled Chern band, at low frequency,

is

$$\rho_\alpha = \begin{bmatrix} i \frac{\omega}{\Delta_\alpha} & -\frac{2\pi}{C_\alpha} \\ \frac{2\pi}{C_\alpha} & i \frac{\omega}{\Delta_\alpha} \end{bmatrix}, \quad (6)$$

where  $\alpha = 1, 2$  is the parton number, and  $\Delta_\alpha$  is proportional to the energy gap of the Chern band filled by the partons  $\alpha$ . In the limit of  $\Delta_\alpha \rightarrow \infty$ , composite fermion theory is reproduced, including the gapped plasma mode and a vanishing electron Drude weight.

The Fermi liquid phase is obtained for  $-\mathcal{C}_1 = \mathcal{C}_2 = 1$ , i.e., when the sum of the Chern numbers of the two partons adds to zero. Then, the combined resistivity of the two parton bands is the resistivity matrix of a superfluid, and the total electron resistivity is dominated by that of the composite fermions. As a consequence, the plasma mode is gapless, and when the gaps  $\Delta_\alpha$  are large, the electronic Drude weight is the same as that of the composite fermions,  $\mathcal{D}_e = \mathcal{D}$ .

Within this framework, a transition from the CFL to the FL requires the Chern number of one of the partons, which we choose to be  $\mathcal{C}_1$ , to change by two. We may envision this to happen in a direct transition or through an intermediate phase with  $\mathcal{C}_1 = 0$ . We first focus on the direct transition. To analyze the electromagnetic responses of the CFL and the FL transition, we do not integrate out  $a_\mu, b_\mu$ , but rather integrate out first the fermionic fields  $d_1$  and  $d_2$ . The effective actions for both bands then depend on the gauge fields  $a_\mu, b_\mu$ . For the  $d_1, d_2$  bands to be gapped at  $\nu = 1/2$ , the flux associated with the Chern-Simons magnetic fields  $\nabla \times \mathbf{a}$  and  $\nabla \times \mathbf{b}$  should be one half of a flux quantum per lattice cell, such that the magnetic unit cell becomes two lattice cells. Then, the effective action for both  $d_1$  and  $d_2$  is that of a full Chern band with a two-fold degeneracy of the spectrum. In the vicinity of the phase transition, the gap closing and Chern number changing of the partons is, in general, described by massive Dirac fermions with masses  $|m_\alpha| \propto \Delta_\alpha$  flipping their sign. Concretely, the continuous transition from the CFL to the FL phase takes place by a band inversion of two massive Dirac fermions with equal mass  $m'_1 = m'_2 \equiv m_1$ . In our conventions,  $m_1 < 0$  corresponds to the CFL phase, and  $m_1 > 0$  to the FL phase. Note that the simultaneous closure of the mass of both fermions is protected by translational symmetry [31], i.e., by the magnetic unit cell being twice the lattice unit cell. Throughout the transition, we assume the gap  $\Delta_2$  to remain large, and the phase transition is only driven by  $\Delta_1$ . At the one-loop level, we express the low-energy effective Lagrangian obtained after integrating out a parton in a gapped Chern insulator in terms of a current-current correlation function, which is a sum of a CS term and a Maxwell term. The explicit expression is presented in the End Matter; see Eqs. (10) and (11).

On the FL side, since  $\mathcal{C}_1 + \mathcal{C}_2 = 0$ , the plasma mode is gapless. Furthermore, near the transition, the electronic Drude weight,  $\mathcal{D}_e^{-1} = \mathcal{D}^{-1} + \Delta_1^{-1}$ , rises continuously from zero when tuning further into the FL phase. On the CFL side, the proximity of the transition affects the plasma mode. For frequencies  $\omega > \Delta_1$ , the resistivity also has a real, dissi-

pative component, originating from inter-parton-band transitions. Thus, close to the critical point, where  $\Delta_1$  is small, the plasma mode becomes damped and acquires a width. In Fig. 1 we present the real part of the conductivity at  $q = 0$  as a function of  $\omega$ , calculated from Eq. (5) for different values of  $\Delta_1$ , parameterized by  $m_1$ . The sharply-defined gapped plasmon is observed at  $m_1 < -\pi\mathcal{D}$ . Its spectral weight is smeared when  $-\pi\mathcal{D} < m_1 < 0$ . The plasmon becomes gapless for positive  $m_1$ , implying a non-zero Drude weight. We remark that our parton theory captures only intra-band processes and neglects electronic transitions to higher Chern bands. As a result, a portion of the spectral weight in the physical response will be transferred to inter-band transitions at higher energies. In our theory, the spectral weight resides entirely in the shown intra-band excitations. The finite spectral weight for intra-band excitations at  $q = 0$  is allowed because we consider a Chern band [59–62], where continuous translation symmetry is broken, which should be contrasted with a Landau level with Galilean invariance.

At the critical point ( $m_1 = 0$ ) we find that the conductivity satisfies an "f-sum rule",  $\lim_{q \rightarrow 0} \int_{-\infty}^{\infty} d\omega \text{Re}[\sigma_{xx}(\omega)] = \pi\mathcal{D}$ , even though we use a relativistic Dirac fermion polarization tensor in composing the electron response function; see Eqs. (15) and (16) in the End Matter for details. However, this should not be understood as the familiar f-sum rule where the integral gives  $\pi \frac{n}{m_e}$  with  $m_e$  the bare mass of electrons, because the  $\mathcal{D}$  we used for the  $f$ -parton Fermi liquid generally depends on the interaction energy scale.

We use free Dirac fermions as the critical theory, which provides a good leading-order approximation. Since we focus on the qualitative behavior at low energies and near the bandgap, we argue that the general features still persist in a more accurate critical theory. Remarkably, the mechanism for plasmon damping is insensitive to the precise values of the critical exponents. Moreover, we expect this damping to happen even when the transition is weakly first-order, since the plasmon damping arises in a finite range around the critical point.

*Other transport signatures.*—Two other physical phenomena whose behavior across the transition we explore are the chirality-selective transmission of light ("chiral mirror"), which occurs at a frequency  $\omega_0$  for which  $\det \sigma_e(\omega_0) = 0$ , and the longitudinal electronic conductivity at  $q \neq 0$ , whose linear dependence on  $q$  is an identifying feature of composite Fermi liquid physics. The first requires us to incorporate the Berry curvature of the composite fermion band into  $\rho_{\text{CF}}$ , while the second requires the incorporation of the wave vector  $q$  into the expressions we derived above.

When the CF band has a finite Berry curvature, and that curvature integrates to a non-zero Hall conductance  $\sigma_{xy}^{\text{CF}}$  in a half-filled band, the CF resistivity becomes

$$\rho_{\text{CF}} = \begin{bmatrix} -i\frac{\mathcal{D}}{\omega} & \sigma_{xy}^{\text{CF}} \\ -\sigma_{xy}^{\text{CF}} & -i\frac{\mathcal{D}}{\omega} \end{bmatrix}^{-1} \quad (7)$$

and its determinant diverges for  $\omega_0 = \mathcal{D}/\sigma_{xy}^{\text{CF}}$ . The reflection and transmission amplitudes  $E_r$  and  $E_t$  of an electromagnetic

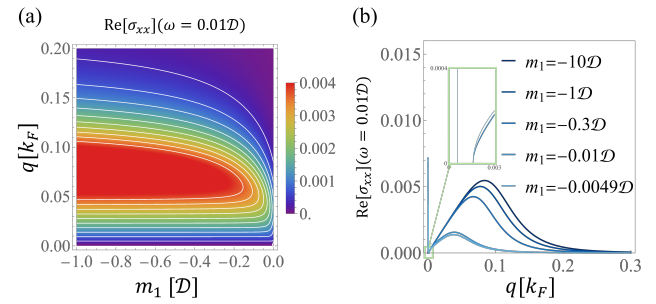


FIG. 2. *Dissipative part of conductivity at finite momentum.* (a) Electron conductivity at  $\omega = 0.01\mathcal{D}$  in CFL ( $m_1 < 0$ ) phase near the phase transition at different wave vectors. The region with a linear in  $q$  conductivity (approximately equal distant contours) is bounded by  $|m_1|$  when  $|m_1|$  is small. (b) Line cuts at different  $m_1$ . The inset shows the behavior at small  $q$  indicated by the green box. When the mass of the Dirac fermion  $m_1$  goes below  $\omega/2$ , we also get a real conductivity at small  $q$  due to the dissipation events from the particle-hole continuum of the almost gapless Dirac fermion parton.

wave of amplitude  $E_0$  incident perpendicular to a (2D) system are closely related to the conductivity matrix  $\sigma_e$

$$E_r = -\frac{1}{1 + \tilde{\alpha}\sigma_e} \tilde{\alpha}\sigma_e E_0 \quad (8)$$

$$E_t = \frac{1}{1 + \tilde{\alpha}\sigma_e} E_0 \quad (9)$$

where  $\tilde{\alpha}$  is the fine structure constant [56, 63, 64]. Consequently, for  $\det \sigma_e(\omega_0) = 0$ , we obtain perfect transmission for one direction of circular polarization (determined by the eigenvector of the zero eigenvalue of  $\sigma_e$ ). The frequency at which that happens,  $\omega_0$ , is continuous across the transition. This is because  $\rho_{1,2}$ , being the resistivities of a full Chern band, are not singular at any frequency. Hence, the chirality-selective transmission originates from the vanishing of the determinant of the conductivity of the  $f$  partons only.

To analyze the electronic conductivity at  $q \neq 0$ , we set  $\sigma_{xy}^{\text{CF}} = 0$  again. A characteristic property of the CFL is that its conductivity is linear in wave vector [46, 65],  $\text{Re} \sigma_{xx} \propto q$ , when  $16\pi^2(q/k_F)^3 < \omega/\mathcal{D} < 4\pi q/k_F$  with  $k_F$  the Fermi momentum. Near the transition, the gap gets small, and  $\rho_{\text{CS}}$  changes dramatically when a transition of a single parton from a full to an empty parton band becomes possible at the wave vector  $q$  and frequency  $\omega$ . Therefore, the breakdown of the linear in  $q$  behavior of  $\text{Re} \sigma_{xx}$  allows us to infer when that happens. This behavior is seen in Fig. (2); see Eqs. (18–21) in the End Matter for details of the calculation.

*Indirect transitions.*—So far, we considered a CFL-FL transition in which one of the bands of  $d_1$  or  $d_2$  goes through a transition between  $\mathcal{C} = +1$  and  $\mathcal{C} = -1$  states. In principle, this transition may be indirect and go through a  $\mathcal{C} = 0$  phase. Such a transition requires breaking of translational symmetry, such that the lattice unit cell is doubled [31, 66]. A full band with  $\mathcal{C} = 0$  is a trivial insulator, for which the resistivity is infinite at zero temperature. Such a band would then dominate the Ioffe-Larkin rule Eq. (5), and lead to a perfectly insulating

state at  $\nu = 1/2$ . The scenario of an indirect transition, however, may also lead to a different outcome. Since Chern bands generally lack electron-hole symmetry around  $\nu = 1/2$ , there is a difference between a parton state of the type we consider when composed of electrons and when composed of holes. In the case of electrons, the electronic resistivity we calculate is the system's electronic resistivity. In the case of holes, the resistivity we calculate should be inverted to a conductivity, which then adds to the conductivity of the full Chern band. Hence, when the resistivity is infinite, the holes have a vanishing conductivity, and the total conductivity becomes that of the full Chern band. Consequently, the intermediate phase, which we call insulator\*, has vanishing longitudinal charge conductivity, but its Hall conductivity may be finite.

While the insulator\* has an infinite charge resistivity at zero temperature due to the infinite resistivity of the  $d_1$  parton, it still carries heat due to the gapless excitations of the  $f$ -partons [23, 67]. Since in the insulator\* phase lattice translational symmetry is broken, the masses of the two Dirac fermions of  $d_1$ ,  $m'_1$ , and  $m''_1$  are generally different. This has consequences on the evolution of the plasma mode in the long wavelength limit across the CFL-insulator\*-FL transition; see Fig. 3(a) and (b). In Fig. 3(a), we show the plasmon behavior near the critical point ( $m'_1 = 0$ ,  $m''_1 < 0$ ) of the CFL-insulator\* TPT, where we change the mass of one of the Dirac fermions ( $m'_1$ ) while keeping the other ( $m''_1 = -15\mathcal{D}$ ) unchanged and keeping  $m_2$  large throughout. The plasmon behavior close to the insulator\*-FL critical point ( $m'_1 > 0$ ,  $m''_1 = 0$ ) is shown in Fig. 3(b), where we change  $m''_1$  while keeping  $m'_1 = 15\mathcal{D}$  unchanged. In the insulator\* phase, we observe two distinct plasma modes, which appear due to the distinct masses  $m'_1 \neq m''_1$ , related to broken translations. While the details vary compared to the simple CFL-FL transition, we find that the plasmon damping behavior is a rather general and robust feature of TPTs.

*Plasma modes in bosonic deconfined TPTs.*—The CFL-FL is only one of several TPTs that may take place within a partially filled Chern band. We now turn to discuss the plasma modes when the Chern band is half-filled with bosons, and the transition is from the Laughlin  $\nu = 1/2$  to a superfluid [25]. In this case, the deconfined TPT theory proposes to fractionize the boson into two fermionic partons,  $b^\dagger = d_1^\dagger d_2^\dagger$ . When both  $d_1$  and  $d_2$  are in insulating states with  $\mathcal{C} = 1$ , the boson is in the Laughlin state. By contrast, when  $d_1$  ( $d_2$ ) is in an insulating state with  $\mathcal{C} = -1$  ( $\mathcal{C} = 1$ ), the corresponding bosonic state is a superfluid. Therefore, the Laughlin-superfluid transition results from a continuous TPT of  $d_1$  from  $\mathcal{C} = 1$  to  $\mathcal{C} = -1$ . The picture is analogous to that of the transition between CFL and FL, as the two transitions are argued to share the same critical theory [23].

The plasma mode of this transition deserves discussion. Deep in the Laughlin state side, when the bands of the two partons are identical, the electronic resistivity is just twice the resistivity matrix of a filled Chern band. A full Chern band has a continuum of interband particle-hole excitations, but no sharp collective plasma mode. This is because the determi-

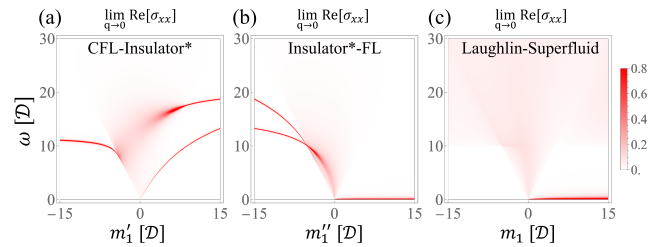


FIG. 3. *Plasmon damping for different deconfined TPTs.* Near the deconfined TPTs, the plasma mode gets damped when entering the particle-hole continuum of the Dirac fermions (fan defined by  $\omega > 2|m_1|$ ), similar to the CFL-FL transition. (a) CFL-insulator\* transition, where one of the Dirac fermions ( $m'_1$ ) flips the sign of the mass, while the other retains a negative mass,  $m''_1 < 0$ . (b) Insulator\*-FL transition, where  $m'_1$  remains positive while  $m''_1$  flips its sign. (c) Laughlin state ( $m_1 < 0$ ) to superfluid ( $m_1 > 0$ ) transition. There is no sharp plasma mode for the Laughlin state.

nant of the resistivity does not vanish at frequencies within the gap, but rather at the threshold of the particle-hole continuum. Near the transition, the gaps of the two bands become very different, and additional continuous particle-hole excitations of the parton with the smaller energy gap become possible. Therefore, no sharp collective mode arises. Between these limiting cases, a sharp plasma mode may occur in principle, but it is not guaranteed to occur. We show the conductivity in Fig. 3(c) using the Dirac cone response functions, leading to a broad continuum instead of a sharp plasma mode for all values of the gaps of the two partons. In the calculations, we assumed the  $d_2$  parton to be a Dirac fermion with mass  $m_2 = -5\mathcal{D}$ .

*Summary & Outlook.*—We discussed the behavior of distinct electromagnetic-response observables across a continuous topological phase transition between a CFL and an FL in the half-filled Chern band, as well as several related transitions. Recent experiments have found indications for a rich landscape of unconventional phases [8–17] and their electromagnetic response can be directly characterized with THz spectroscopy [51–55]. Our discussion was based on two premises – the addition of resistivities of the three partons, which is a defining feature of a parton system, and the description of the partons  $d_1$  and  $d_2$  in terms of massive Dirac fermions. The second premise is approximate, but its central features, in particular the behavior of the response functions for  $\omega$  close to zero and close to the energy gap are a consequence of general considerations.

For future work, it will be interesting to numerically study the transition and quantitatively predict the spectral weights of the conductivity in concrete settings. In addition, the formalism we develop allows us to predict the electromagnetic response away from a filling of  $\nu = 1/2$ , where a rich landscape of topological phases and exotic phase transitions may arise. In particular, superconductivity has been predicted to appear in the vicinity of topological phase transitions [35, 42–44], whose electromagnetic response would be interesting to study.

*Acknowledgements.*—We thank Long Ju, Zach Hadjri, and Clemens Kuhlenkamp for fruitful discussions. X.Y. thanks Wei Ku, Tingxin Li, Guorui Chen, and Xiaoxue Liu for helpful discussions and Xin Liu at TDLI for hospitality, where this work was initiated. We acknowledge support from the Israeli Science Foundation, the Israeli Ministry of Science Technology and Space, the Minerva Stiftung, the DFG (CRC/Transregio 183, EI 519/7-1), the Israel Science Foundation ISF (Grant No 1914/24), ISF Quantum Science and Technology (2074/19), from the Deutsche Forschungsgemeinschaft (DFG, German Research Foundation) under Germany’s Excellence Strategy-EXC-2111-390814868, TRR 360 – 492547816 and DFG grants No. KN1254/1-2, KN1254/2-1, the European Union (grant agreement No. 101169765), as well as the Munich Quantum Valley (MQV), which is supported by the Bavarian state government with funds from the Hightech Agenda Bayern Plus.

*Data availability.*—All data is contained in this manuscript.

## End Matter

### Current-current response function

To calculate the conductivity and resistivity of the  $d_1$  parton described by two degenerate massive Dirac fermions, we first compute the effective Lagrangian near the TPT. On a one-loop level, we find

$$\mathcal{L}_1[a_\mu] = \frac{1}{2} a_\mu \Pi_{\mu\nu} a_\nu, \quad (10)$$

where the current-current response function of massive Dirac fermions  $\Pi_{\mu\nu} = \Pi_{\mu\nu}^{\text{MW}} + \Pi_{\mu\nu}^{\text{CS}}$  is composed of a Maxwell and Chern-Simons term, given by

$$\begin{aligned} \Pi_{\mu\nu}^{\text{MW}} &= \frac{1}{4\pi} (-\eta_{\mu\nu} q_\alpha q^\alpha + q_\mu q_\nu) \frac{1}{q_E^3} \left( 2q_E|m| - (4m^2 - q_E^2) \arctan\left(\frac{q_E}{2|m|}\right) \right) \\ \Pi_{\mu\nu}^{\text{CS}} &= -\frac{im}{2\pi} \epsilon_{\mu\lambda\nu} q^\lambda \frac{2}{q_E} \arctan\left(\frac{q_E}{2|m|}\right) \end{aligned} \quad (11)$$

with the Dirac velocity set to one for simplicity,  $\eta_{\mu\nu} = \text{diag}(1, -1, -1)$ ,  $q_E = \sqrt{-\omega^2 + \mathbf{q}^2}$ , and  $m$  the mass of Dirac fermion. We choose the UV regularizations for the two Dirac fermions so that there is no extra CS term. Similar expressions hold for the second parton, with  $a_\mu$  being replaced by  $b_\mu$  and the mass changed to the  $d_2$  parton band gap accordingly.

In the Coulomb gauge, where  $\mathbf{q} \cdot \mathbf{a} = \mathbf{q} \cdot \mathbf{b} = 0$ , and for  $\mathbf{q} \parallel \hat{\mathbf{x}}$ , the correlation function reduces to

$$\Pi_{\mu\nu} = \begin{bmatrix} \Pi_{00} & \Pi_{0y} \\ \Pi_{y0} & \Pi_{yy} \end{bmatrix} \quad (12)$$

From the continuity equation, it follows that the polarization operator  $\Pi$  is related to the resistivity matrices  $\rho$  by

$$\rho = \begin{bmatrix} \sqrt{\frac{iq^2}{\omega}} & 0 \\ 0 & \sqrt{i\omega} \end{bmatrix} \Pi^{-1} \begin{bmatrix} \sqrt{\frac{iq^2}{\omega}} & 0 \\ 0 & \sqrt{i\omega} \end{bmatrix}. \quad (13)$$

Note that the components of the resistivity matrices referred to the spatial  $x$ - and  $y$ -directions, while the components of  $\Pi$  refer to temporal and spatial  $y$  indices as in Eq. (12).

The electronic response function  $\Pi_e$ , i.e., the response function to the electromagnetic field  $A_\mu$ , is obtained by integrating out the fields  $a_\mu, b_\mu$

$$\Pi_e^{-1} = \Pi_f^{-1} + \Pi_1^{-1} + \Pi_2^{-1}. \quad (14)$$

with  $\Pi_\alpha$  being the response function of the  $d_\alpha$  parton, and  $\Pi_f$  being the response function of the  $f$ -parton. Together with Eq. (13), this relation leads to the Ioffe-Larkin rule Eq. (5).

In the low-frequency and long-wavelength limit,  $m^2 \gg q^2, \omega^2$ , the polarization operator  $\Pi_{\mu\nu}$  is dominated by the CS term,  $\frac{C}{4\pi}ada$  with  $C = -1$  ( $C = 1$ ) for  $m > 0$  ( $m < 0$ ), corresponding to a Hall conductance of  $\pm 1$ . When that is the case, the  $a_0$  terms in (4) enforce the constraints  $\nabla \times \mathbf{a} = C_1 d_1^\dagger d_1$  and  $\nabla \times \mathbf{b} = C_2 d_2^\dagger d_2$ . Then, when  $C_1 = C_2 = 1$ , the  $f$ -partons experience a magnetic field corresponding to two flux quanta per electron, making the  $f$ -partons composite fermions. Since  $\nu = 1/2$ , this field corresponds to one flux quantum per lattice unit cell, such that the magnetic unit cell and the lattice unit cell coincide and the  $f$  parton remains a gapless FL state. The electron system then forms a CFL.

The diagonal term of  $\Pi$  is translated by Eq. (13) to an imaginary diagonal resistivity that is proportional to  $\omega$  at low frequencies, and approaches a constant as  $\omega$  approaches the energy gap, where it also acquires a real, dissipative part. The linear dependence of the diagonal conductivity on  $i\omega$  holds for small  $\omega$  for all gapped systems. The details of its evolution for frequencies well within the gap depend on the details of the band structure, which are not captured by the effective Dirac cone model.

For  $m_1 = 0$ , at the phase transition, the parton  $d_1$  Lagrangian includes only the Maxwell term  $\frac{1}{8} (-\eta_{\mu\nu} q_\alpha q^\alpha + q_\mu q_\nu) \frac{1}{q_E}$ . In the long-wavelength limit  $q \rightarrow 0$  we set  $\omega \rightarrow \omega + i\delta$  with  $\delta$  infinitesimal to get the retarded function  $[\Pi_1]_{00} = \frac{1}{8} \frac{|\vec{q}|^2}{-\omega}$ . For two gapless Dirac fermions, this gives the well-known constant optical conductivity of the  $d_1$  partons via  $\sigma_{xx}(\omega) = \frac{\omega}{i|\vec{q}|^2} \Pi_{00} = \frac{1}{8}$  and the electronic

current-current response reduces to

$$\Pi^e = \frac{1}{(\frac{\omega}{\mathcal{D}} + 8i)^2 - 4\pi^2} \begin{bmatrix} -(\frac{1}{\mathcal{D}} + \frac{8i}{\omega})q^2 & -2\pi iq \\ 2\pi iq & -(\frac{\omega^2}{\mathcal{D}} + 8i\omega) \end{bmatrix}. \quad (15)$$

The real part of the longitudinal conductivity at small  $\omega$  is then

$$\lim_{\omega \rightarrow 0} \text{Re}[\sigma_{xx}^e] = \frac{2}{16 + \pi^2}, \quad (16)$$

which agrees with the linecuts shown in Fig. 1(b).

Eqs. (11) and (14) are what is needed for the analysis of the transport properties we discussed in the main text, and their behavior when tuning through the phase transition. The plasmon and the Drude weight are directly obtained from these expressions by setting  $q \rightarrow 0$ , and using Eq. (13) to obtain the resistivity. The plasmon is a sharp mode when the diagonal element of the resistivity is purely imaginary, and the Hall element is real. This requires the frequency of the mode to be within the gap of the two parton bands. Close to the transition, this condition ceases to hold, and the plasmon gets damped.

### Drude weight and $q$ -dependent conductivity

We now calculate the Drude weight and the  $q$ -dependent conductivity close to the CFL-FL transition.

A characteristic quantity of the FL is the electronic Drude weight,  $\mathcal{D}_e = \lim_{\omega \rightarrow 0} i\omega \sigma_e(q = 0, \omega)$ , with  $\sigma_e \equiv \rho_e^{-1}$  being the electronic conductivity, in the absence of impurity scattering. We start from the FL ( $m_1 > 0$ ) side, in the low frequency limit,  $m_1 \gg \omega \gg q$ , we have  $\Pi_1 = \frac{1}{12\pi m_1} \begin{bmatrix} q^2 & 0 \\ 0 & \omega^2 \end{bmatrix} + \frac{1}{2\pi} \begin{bmatrix} 0 & -iq \\ iq & 0 \end{bmatrix}$ . This leads to an electron po-

larization

$$\Pi_e = -\frac{1}{\frac{1}{\mathcal{D}} + \frac{\pi}{3m_1}} \begin{bmatrix} \frac{q^2}{\omega^2} & 0 \\ 0 & 1 \end{bmatrix} \quad (17)$$

which describes an FL with Drude weight  $\frac{1}{\frac{1}{\mathcal{D}} + \frac{\pi}{3m_1}}$ . We find the Drude weight saturates at  $\mathcal{D}$  for large  $m_1$  and decreases continuously to zero as  $m_1 \rightarrow 0$ . The linear decrease of Drude weight at small  $m_1$  is a result of a free Dirac fermion, which could possibly be modified by the critical theory

A unique property of the CFL phase is the wave vector-dependent conductivity  $\text{Re} \sigma_{xx} \propto q$  for  $16\pi^2(q/k_F)^3 < \omega/\mathcal{D} < 4\pi q/k_F$  with  $k_F$  the Fermi momentum. To extract the linear in  $q$  conductivity in the CFL ( $m < 0$ ) phase, we need the polarization tensors for  $16\pi^2(q/k_F)^3 < \omega/\mathcal{D} < 4\pi q/k_F$ . In this limit, the  $f$  Fermi liquid contributes

$$\Pi_f \approx \begin{bmatrix} \frac{k_F^2}{8\pi^2 \mathcal{D}} & 0 \\ 0 & \frac{i\omega k_F}{2\pi q} \end{bmatrix}. \quad (18)$$

When  $q \ll |m_1|$ , the  $d_1$  Dirac fermions contribute

$$\Pi_1 = \begin{bmatrix} \frac{q^2}{12\pi|m_1|} & \frac{iq}{2\pi} \\ -\frac{iq}{2\pi} & -\frac{q^2}{12\pi|m_1|} \end{bmatrix} \quad (19)$$

and we arrive at the linear in  $q$  conductivity  $\sigma_{xx}(q, \omega) = \frac{q}{2\pi k_F}$ , while for  $q \gg |m_1|$  we find

$$\Pi_1 = \begin{bmatrix} \frac{q}{16} & -i\frac{m_1}{4} \\ i\frac{m_1}{4} & -\frac{q}{16} \end{bmatrix}, \quad (20)$$

which gives us

$$\sigma_{xx}(q, \omega) = \frac{i\omega (\pi (16m_1^2 - q^2) - 8i\omega k_F)}{(16q + 8\pi^2 \mathcal{D} \frac{q^2}{k_F^2}) (\pi q^2 + 8ik_F \omega) + 128\pi^2 \mathcal{D} m_1^2 \frac{q^2}{k_F^2}} \quad (21)$$

with a complicated  $(q, \omega)$  dependence. Thus, the linear in  $q$  conductivity  $\sigma_{xx}$  terminates at around scale  $q_c \sim |m_1|$  as shown in Fig. 2. Starting from a large Dirac fermion mass  $m_1$ , when  $4\pi \mathcal{D} q/k_F > \omega$ , we get a real part of conductivity from the particle-hole continuum of the  $f$  parton Fermi liquid and when  $16\pi^2 \mathcal{D} (q/k_F)^3 \ll \omega$ ,  $\text{Re} \sigma_{xx} \propto q$ . When the gap of the Dirac fermion,  $2m$ , gets below  $\omega$ , we get additional real conductivity at small  $q$  from the dissipation channels of the Dirac fermions.

### Plasma modes in the bosonic Laughlin and insulator\* phases

In this section, we discuss the behavior of plasma modes in the bosonic Laughlin  $\nu = 1/2$  state and insulator\* phase. For the bosonic  $\nu = 1/2$  Laughlin state, we find that there is no sharp plasma mode, just as in the case of a fermionic fully-filled Chern band. This is because here the plasmon frequency is higher than the gap of the  $d_2$  parton, and therefore it is damped even far from the phase transition.

For the insulator\* phase, where the two Dirac cones of the  $d_1$  parton have two different masses, we find two plasma modes. The easiest way to understand this finding is from looking at the polarization tensor when the masses of the Dirac fermions are opposite  $m'_1 = -m''_1$ .

In this case, the polarization tensor for  $d_1$  parton behaves as  $\Pi_1 = \frac{1}{12\pi|m'_1|} \begin{bmatrix} q^2 & 0 \\ 0 & \omega^2 \end{bmatrix}$ , together with the contribution  $\Pi_f = -\mathcal{D} \begin{bmatrix} \frac{q^2}{\omega^2} & 0 \\ 0 & 1 \end{bmatrix}$  from  $f$  parton and  $\Pi_2 = \frac{1}{2\pi} \begin{bmatrix} 0 & iq \\ -iq & 0 \end{bmatrix}$  from  $d_2$  parton. We note that in this limit, the signs of the polarization tensor of the  $d_1$  parton and the  $d_2$  parton are different. Physically, this arises from the different responses of metals and insulators to an external electric field. For a metal, the quasiparticles have a mass, and therefore the current response to the external electric field is delayed, which corresponds to a positive imaginary part of the conductivity. On the other hand, for an insulator, a low-frequency electric field induces a polarization, and the current is the time derivative of this polarization, which corresponds to a negative imaginary conductivity. The plasmon frequencies are then determined by  $\det \Pi_e^{-1} = 0$ , which further reduces to  $\left| \frac{12\pi|m'_1|}{\omega} - \frac{\omega}{\mathcal{D}} \right| = 2\pi$ ; an equation that has two positive solutions  $\omega_{p1,2}$ . These considerations also hold more generally for different masses of the Dirac fermions  $m'_1 \neq m'_2$ .

---

[1] M. Hafezi, A. S. Sørensen, E. Demler, and M. D. Lukin, Fractional quantum hall effect in optical lattices, *Phys. Rev. A* **76**, 023613 (2007).

[2] E. Kapit and E. Mueller, Exact Parent Hamiltonian for the Quantum Hall States in a Lattice, *Physical Review Letters* **105**, 215303 (2010), publisher: American Physical Society.

[3] T. Neupert, L. Santos, C. Chamon, and C. Mudry, Fractional Quantum Hall States at Zero Magnetic Field, *Physical Review Letters* **106**, 236804 (2011), publisher: American Physical Society.

[4] X.-L. Qi, Generic Wave-Function Description of Fractional Quantum Anomalous Hall States and Fractional Topological Insulators, *Physical Review Letters* **107**, 126803 (2011), publisher: American Physical Society.

[5] N. Regnault and B. A. Bernevig, Fractional Chern Insulator, *Physical Review X* **1**, 021014 (2011), publisher: American Physical Society.

[6] D. N. Sheng, Z.-C. Gu, K. Sun, and L. Sheng, Fractional quantum Hall effect in the absence of Landau levels, *Nature Communications* **2**, 389 (2011), publisher: Nature Publishing Group.

[7] E. Tang, J.-W. Mei, and X.-G. Wen, High-Temperature Fractional Quantum Hall States, *Physical Review Letters* **106**, 236802 (2011), publisher: American Physical Society.

[8] J. Cai, E. Anderson, C. Wang, X. Zhang, X. Liu, W. Holtzmann, Y. Zhang, F. Fan, T. Taniguchi, K. Watanabe, Y. Ran, T. Cao, L. Fu, D. Xiao, W. Yao, and X. Xu, Signatures of Fractional Quantum Anomalous Hall States in Twisted MoTe<sub>2</sub> Bilayer, *Nature* **622**, 63 (2023).

[9] H. Park, J. Cai, E. Anderson, Y. Zhang, J. Zhu, X. Liu, C. Wang, W. Holtzmann, C. Hu, Z. Liu, T. Taniguchi, K. Watanabe, J.-H. Chu, T. Cao, L. Fu, W. Yao, C.-Z. Chang, D. Cobden, D. Xiao, and X. Xu, Observation of fractionally quantized anomalous Hall effect, *Nature* **622**, 74 (2023).

[10] F. Xu, Z. Sun, T. Jia, C. Liu, C. Xu, C. Li, Y. Gu, K. Watanabe, T. Taniguchi, B. Tong, J. Jia, Z. Shi, S. Jiang, Y. Zhang, X. Liu, and T. Li, Observation of Integer and Fractional Quantum Anomalous Hall Effects in Twisted Bilayer MoTe<sub>2</sub>, *Physical Review X* **13**, 031037 (2023).

[11] Y. Zeng, Z. Xia, K. Kang, J. Zhu, P. Knüppel, C. Vaswani, K. Watanabe, T. Taniguchi, K. F. Mak, and J. Shan, Thermodynamic evidence of fractional Chern insulator in moiré MoTe<sub>2</sub>, *Nature* **622**, 69 (2023).

[12] F. Xu, Z. Sun, J. Li, C. Zheng, C. Xu, J. Gao, T. Jia, K. Watanabe, T. Taniguchi, B. Tong, L. Lu, J. Jia, Z. Shi, S. Jiang, Y. Zhang, Y. Zhang, S. Lei, X. Liu, and T. Li, *Signatures of unconventional superconductivity near reentrant and fractional quantum anomalous Hall insulators* (2025), arXiv:2504.06972 [cond-mat].

[13] F. Liu, F. Xu, C. Xu, J. Li, Z. Sun, J. Xiao, N. Mao, X. Chang, X. Tao, K. Watanabe, T. Taniguchi, J. Jia, R. Zhong, Z. Shi, S. Wang, G. Chen, X. Liu, D. Qian, Y. Zhang, T. Li, and S. Jiang, *From fractional chern insulators to topological electronic crystals in moiré MoTe<sub>2</sub>: quantum geometry tuning via remote layer* (2025), arXiv:2512.03622 [cond-mat.mes-hall].

[14] Z. Lu, T. Han, Y. Yao, A. P. Reddy, J. Yang, J. Seo, K. Watanabe, T. Taniguchi, L. Fu, and L. Ju, Fractional quantum anomalous Hall effect in multilayer graphene, *Nature* **626**, 759 (2024).

[15] T. Han, Z. Lu, Y. Yao, J. Yang, J. Seo, C. Yoon, K. Watanabe, T. Taniguchi, L. Fu, F. Zhang, and L. Ju, Large quantum anomalous Hall effect in spin-orbit proximitized rhombohedral graphene, *Science* **384**, 647 (2024).

[16] T. Han, Z. Lu, Z. Hadjri, L. Shi, Z. Wu, W. Xu, Y. Yao, A. A. Cotten, O. Sharifi Sede, H. Weldeyesus, J. Yang, J. Seo, S. Ye, M. Zhou, H. Liu, G. Shi, Z. Hua, K. Watanabe, T. Taniguchi, P. Xiong, D. M. Zumbühl, L. Fu, and L. Ju, Signatures of chiral superconductivity in rhombohedral graphene, *Nature* **643**, 654 (2025).

[17] Z. Lu, T. Han, Y. Yao, Z. Hadjri, J. Yang, J. Seo, L. Shi, S. Ye, K. Watanabe, T. Taniguchi, and L. Ju, Extended quantum anomalous Hall states in graphene/hBN moiré superlattices, *Nature* **1** (2025).

[18] X.-G. Wen and Y.-S. Wu, Transitions between the quantum Hall states and insulators induced by periodic potentials, *Physical Review Letters* **70**, 1501 (1993).

[19] W. Chen, M. P. A. Fisher, and Y.-S. Wu, Mott transition in an anyon gas, *Physical Review B* **48**, 13749 (1993).

[20] A. W. W. Ludwig, M. P. A. Fisher, R. Shankar, and G. Grinstein, Integer quantum Hall transition: An alternative approach and exact results, *Physical Review B* **50**, 7526 (1994).

[21] J. Ye and S. Sachdev, Coulomb Interactions at Quantum Hall Critical Points of Systems in a Periodic Potential, *Physical Review Letters* **80**, 5409 (1998).

[22] X.-G. Wen, Continuous Topological Phase Transitions between Clean Quantum Hall States, *Physical Review Letters* **84**, 3950 (2000).

[23] M. Barkeshli and J. McGreevy, Continuous transitions between composite Fermi liquid and Landau Fermi liquid: A route to fractionalized Mott insulators, *Physical Review B* **86**, 075136 (2012).

[24] T. Grover and A. Vishwanath, Quantum phase transition between integer quantum Hall states of bosons, *Physical Review B* **87**, 045129 (2013).

[25] M. Barkeshli and J. McGreevy, Continuous transition between fractional quantum Hall and superfluid states, *Physical Review B* **89**, 235116 (2014).

[26] T. Grover, Entanglement Monotonicity and the Stability of Gauge Theories in Three Spacetime Dimensions, *Physical Review Letters* **112**, 151601 (2014).

[27] M. Barkeshli, N. Yao, and C. Laumann, Continuous Preparation of a Fractional Chern Insulator, *Physical Review Letters* **115**, 026802 (2015).

[28] J. Y. Lee, C. Wang, M. P. Zaletel, A. Vishwanath, and Y.-C. He, Emergent Multi-Flavor QED 3 at the Plateau Transition between Fractional Chern Insulators: Applications to Graphene Heterostructures, *Physical Review X* **8**, 031015 (2018).

[29] R. Ma and Y.-C. He, Emergent  $\{QCD\}_3$  quantum phase transitions of fractional Chern insulators, *Physical Review Research* **2**, 033348 (2020).

[30] X.-Y. Song and Y.-H. Zhang, Deconfined criticalities and dualities between chiral spin liquid, topological superconductor and charge density wave Chern insulator, *SciPost Physics* **15**, 215 (2023).

[31] X.-Y. Song, Y.-H. Zhang, and T. Senthil, Phase transitions out of quantum Hall states in moiré materials, *Physical Review B* **109**, 085143 (2024).

[32] B. Han and D. F. Mross, Exotic phase transitions in spin ladders with discrete symmetries that emulate spin-1/2 bosons in two dimensions (2024), arXiv:2412.17911 [cond-mat].

[33] C. Kuhlenkamp, W. Kadow, A. İmamoğlu, and M. Knap, Chiral pseudospin liquids in moiré heterostructures, *Phys. Rev. X* **14**, 021013 (2024).

[34] S. Divic, T. Soejima, V. Crépel, M. P. Zaletel, and A. Millis, Chiral spin liquid and quantum phase transition in the triangular lattice hofstadter-hubbard model (2025), arXiv:2406.15348 [cond-mat.str-el].

[35] S. Divic, V. Crépel, T. Soejima, X.-Y. Song, A. J. Millis, M. P. Zaletel, and A. Vishwanath, Anyon superconductivity from topological criticality in a hofstadter-hubbard model, *Proceedings of the National Academy of Sciences* **122**, e2426680122 (2025), <https://www.pnas.org/doi/pdf/10.1073/pnas.2426680122>.

[36] H. Lu, H.-Q. Wu, B.-B. Chen, and Z. Y. Meng, Continuous Transition between Bosonic Fractional Chern Insulator and Superfluid, *Physical Review Letters* **134**, 076601 (2025).

[37] T. Lotrič and S. H. Simon, Paired Parton Trial States for the Superfluid-Fractional Chern Insulator Transition (2025), arXiv:2504.20139 [cond-mat].

[38] T. Wang, X.-Y. Song, M. P. Zaletel, and T. Senthil, Emergent  $QED_3$  at the bosonic Laughlin state to superfluid transition (2025), arXiv:2507.07611 [cond-mat].

[39] Z. Zhou, C. Wang, and Y.-C. He, Chern-Simons-matter conformal field theory on fuzzy sphere: Confinement transition of Kalmeyer-Laughlin chiral spin liquid (2025), arXiv:2507.19580 [cond-mat].

[40] Y.-H. Zhang, Continuous transition from Fermi liquid to A fractional Chern insulator (2025), arXiv:2507.22130 [cond-mat].

[41] Q. Zhang and W.-T. Xu, Continuous topological phase transition between  $z_2$  topologically ordered phases (2025), arXiv:2508.08376 [cond-mat].

[42] F. Pichler, C. Kuhlenkamp, M. Knap, and A. Vishwanath, Microscopic mechanism of anyon superconductivity emerging from fractional Chern insulators, *Newton* **10.1016/j.newton.2025.100340**.

[43] C. Kuhlenkamp, S. Divic, M. P. Zaletel, T. Soejima, and A. Vishwanath, Robust superconductivity upon doping chiral spin liquid and chern insulators in a hubbard-hofstadter model (2025), arXiv:2509.02675 [cond-mat.str-el].

[44] F. Chen, W. O. Wang, J.-X. Zhang, L. Balents, and D. N. Sheng, Topological chiral superconductivity in the triangular-lattice hofstadter-hubbard model (2025), arXiv:2509.02757 [cond-mat.str-el].

[45] Y. Zhang, L. Shackleton, and T. Senthil, Pathways from a chiral superconductor to a composite fermi liquid (2025), arXiv:2509.21591 [cond-mat.str-el].

[46] B. I. Halperin, P. A. Lee, and N. Read, Theory of the half-filled Landau level, *Physical Review B* **47**, 7312 (1993).

[47] A. Abouelkomsan, K. Yang, and E. J. Bergholtz, Quantum metric induced phases in Moiré materials, *Physical Review Research* **5**, L012015 (2023).

[48] J. Dong, J. Wang, P. J. Ledwith, A. Vishwanath, and D. E. Parker, Composite Fermi Liquid at Zero Magnetic Field in Twisted MoTe 2, *Physical Review Letters* **131**, 136502 (2023).

[49] H. Goldman, A. P. Reddy, N. Paul, and L. Fu, Zero-field composite fermi liquid in twisted semiconductor bilayers, *Phys. Rev. Lett.* **131**, 136501 (2023).

[50] A. Abouelkomsan, N. Paul, A. Stern, and L. Fu, Compressible Quantum Liquid with Vanishing Drude Weight, *Physical Review Letters* **134**, 176501 (2025), publisher: American Physical Society.

[51] S. Xu, Y. Li, R. A. Vitalone, R. Jing, A. J. Sternbach, S. Zhang, J. Ingham, M. Delor, J. W. McIver, M. Yankowitz, R. Queiroz, A. J. Millis, M. M. Fogler, C. R. Dean, A. N. Pasupathy, J. Hone, M. Liu, and D. N. Basov, Electronic interactions in dirac fluids visualized by nano-terahertz spacetime interference of electron-photon quasiparticles, *Science Advances* **10**, eado5553 (2024), <https://www.science.org/doi/pdf/10.1126/sciadv.ado5553>.

[52] S.-D. Chen, Q. Feng, W. Zhao, R. Qi, Z. Zhang, D. Abeysinghe, C. Uzundal, J. Xie, T. Taniguchi, K. Watanabe, and F. Wang, Direct Measurement of Terahertz Conductivity in a Gated Monolayer Semiconductor, *Nano Letters* **25**, 7998 (2025).

[53] S.-D. Chen, R. Qi, H.-L. Kim, Q. Feng, R. Xia, D. Abeysinghe, J. Xie, T. Taniguchi, K. Watanabe, D.-H. Lee, and F. Wang, Terahertz electrodynamics in a zero-field Wigner crystal (2025), arXiv:2509.10624 [cond-mat].

[54] A. T. Pierce, C. Vaswani, D. Pimenov, S. Xu, K. Watanabe, T. Taniguchi, E. Mueller, D. Chowdhury, K. F. Mak, and J. Shan, Imaging propagating terahertz collective modes in two-dimensional semiconductor double layers (2025), arXiv:2511.22962 [cond-mat.mes-hall].

[55] S. Xu, B. Yang, N. Verma, R. A. Vitalone, B. Vermilyea, M. S. Sánchez, J. Ingham, R. Jing, Y. Shao, T. Stauber, A. Rubio, M. Delor, M. Liu, M. M. Fogler, C. R. Dean, A. Millis, R. Queiroz, and D. N. Basov, Plasmon dynamics in graphene (2026), arXiv:2601.10493 [cond-mat.mes-hall].

[56] A. Stern and L. Fu, Transport Properties of a Half-Filled Chern Band at the Electron and Composite Fermion Phases, *Physical Review Letters* **133**, 246602 (2024).

[57] J. K. Jain, *Composite Fermions* (Cambridge University Press, Cambridge, 2007).

[58] B. I. Halperin and J. K. Jain, *Fractional quantum hall effects* (WORLD SCIENTIFIC, 2020) tex.eprint: <https://www.worldscientific.com/doi/pdf/10.1142/11751>.

[59] F. Wu and A. H. MacDonald, Moiré assisted fractional quantum hall state spectroscopy, *Phys. Rev. B* **94**, 241108 (2016).

[60] N. Paul, A. Abouelkomsan, A. Reddy, and L. Fu, Shining light on collective modes in moiré fractional Chern insulators (2025), arXiv:2502.17569 [cond-mat].

[61] X. Shen, C. Wang, X. Hu, R. Guo, H. Yao, C. Wang, W. Duan, and Y. Xu, Magnetorotons in Moiré Fractional Chern Insulators (2025), arXiv:2412.01211 [cond-mat].

[62] B. M. Kousa, N. Morales-Durán, T. M. R. Wolf, E. Khalaf, and A. H. MacDonald, Theory of magnetoroton bands in moiré materials (2025), arXiv:2502.17574 [cond-mat.mes-hall].

[63] W.-K. Tse and A. H. MacDonald, Magneto-optical Faraday and Kerr effects in topological insulator films and in other layered

quantized Hall systems, *Physical Review B* **84**, 205327 (2011), publisher: American Physical Society.

[64] J. Liu and X. Dai, Anomalous Hall effect, magneto-optical properties, and nonlinear optical properties of twisted graphene systems, *npj Computational Materials* **6**, 57 (2020), publisher: Nature Publishing Group.

[65] R. L. Willett, R. R. Ruel, M. A. Paalanen, K. W. West, and L. N. Pfeiffer, Enhanced finite-wave-vector conductivity at multiple even-denominator filling factors in two-dimensional electron systems, *Physical Review B* **47**, 7344 (1993).

[66] M. Barkeshli and X.-G. Wen, Anyon Condensation and Continuous Topological Phase Transitions in Non-Abelian Fractional Quantum Hall States, *Physical Review Letters* **105**, 216804 (2010).

[67] P. A. Lee and N. Nagaosa, Gauge theory of the normal state of high-  $T_c$  superconductors, *Physical Review B* **46**, 5621 (1992).